A Novel Nonparaxial Time-Domain Beam-Propagation Method for Modeling Ultrashort Pulses in Optical Structures

Husain M. Masoudi

***Abstract*—In this paper, a new nonparaxial time-domain beam-propagation method (TD–BPM) based on Padé approximant for modeling ultrashort optical pulses has been proposed and verified. The high efficiency of the technique in modeling long device interaction comes from solving the TD wave equation along one direction and allowing the time window to follow the evolution of the pulse. The accuracy of the method was tested in three different environments of homogenous and nondispersive medium, metallic, and dielectric waveguides and then was applied to model ultrashort pulse propagation in a directional-coupler device. The characterization of the technique shows excellent performance in terms of accuracy, efficiency, and stability, which the conventional paraxial TD–BPM failed to achieve. The new TD–BPM is particularly well suited for the study of unidirectional propagation of compact ultrashort temporal pulses over long distances in waveguide structures.**

***Index Terms*—Beam propagation method (BPM), finite-difference (FD) analysis, modeling, numerical analysis, optical waveguide theory, Padé approximant, partial differential equation, ultrashort pulse propagation.**

I. Introduction

OPTICAL-communication-circuit designs are moving toward integrating a large number of devices on a single substrate. This process creates new difficulties in understanding the complicated interaction behavior between circuit elements and in improving the efficiency of these circuits. In this context, modeling plays a very important role that helps solve these complexities. On the other hand, there are also a number of challenges in modeling today's and future optical-communication circuits. The first challenge is the fact that most of these devices are designed based on time-domain (TD) interaction rather than continuous wave (CW), where the analysis of TD are much more complicated than CW analysis due to the involvement of a large number of frequency spectra. Unfortunately, most of the techniques developed in the literature are for CW operations, and very few are for the TD study. The second challenge is that most of these circuits involve a large number of elements that have different geometries of 3-D guidance mechanisms, and sometimes, they are designed on nonlinear optical interaction of $\chi^{(2)}$ or $\chi^{(3)}$ responses of the material. The third challenge, and maybe the most difficult, is that most of these devices are designed for interaction over long optical distances, usually on the order of thousands of wavelengths. Accordingly, modeling techniques have to be very efficient and must run easily on ordinary computer resources; otherwise, they are less useful if they require a special computer, such as supercomputers, to which very few people have access. The finite-difference TD (FDTD) is a well-known technique developed and used in many applications to model both TD and CW problems, but it requires huge computer resources, and more importantly, it is not suited for long optical-pulse interaction [1]–[8]. Over the past few years, there have been many attempts to develop new TD techniques to solve these problems [9]–[17]. It was observed that the majority of these techniques are very similar in their approach to the original FDTD. They can be classified in two categories. The first category is called slowly varying envelope methods, where the stepping mechanism uses the first-order time derivative after neglecting the second-order derivative [9]–[14]. Clearly, these techniques are not suited for short optical-pulse propagation. As a matter of fact, they are more suited to CW analysis than TD. The second category is similar to the first group in its standard approach; however, they use higher order approximation, such as Padé relations, to account for the neglected second derivative of time [15]–[17]. Unfortunately, most of these techniques proved to be inferior to FDTD in terms of computer-resource consumption [17]. One-way propagation techniques, such as the beam-propagation method (BPM), are well suited for long device interaction [18]–[21]. However, most of the BPMs were developed for CW operations. Previously, we proposed two paraxial TD–BPM techniques to model optical-pulse propagation in waveguide structures [22], [23]. The techniques are based on an explicit FD (EFD) approach [24], [25], and they proved to be very efficient in modeling optical-pulse propagation in long device interaction. The same EFD approaches were also used efficiently in modeling long CW nonlinear-wave interaction [26], [27]. On the other hand, the parabolic TD–BPM in [22] and [23] showed limitation in modeling ultrashort pulses due to the paraxial approximation involved.

Manuscript received March 29, 2007; revised June 24, 2007. This work was supported by King Fahd University of Petroleum and Minerals (KFUPM), Dhahran, Saudi Arabia, and in part by King Abdul-Aziz City for Science and Technology (KACST), Riyadh, Saudi Arabia.

The author is temporarily with the Emerging Communications Technology Institute, Electrical and Computer Engineering Department, University of Toronto, Toronto, ON M5S 3G4, Canada, and he is permanently with the Department of Electrical Engineering, King Fahd University of Petroleum and Minerals, Dhahran 31261, Saudi Arabia (e-mail: husainm@kfupm.edu.sa).

Color versions of one or more of the figures in this paper are available online at http://ieeexplore.ieee.org.

Digital Object Identifier 10.1109/JLT.2007.904425

One has to notice that modeling ultrashort pulses is difficult due to the fast variation of the pulse envelope during propagation. Based on the same principle, another technique has recently been developed using the finite-element method to model short pulses [28]. The method uses Padé recurrence approximation with the negligence of a few operator derivatives. In addition, there are a few reported techniques in the literature proposed for TD solution of higher order parabolic equations in nonoptical fields, such as seismology and underwater acoustics (see [29] and [30] and some of the references in [31]).

In this paper, we propose a new nonparaxial TD–BPM using the same approach of the paraxial TD–BPM given in [22] and [23]. The new TD–BPM involves writing the TD wave equation as a one-way equation for propagation along the axial direction z while keeping all time variations intact by treating them as another transverse variable, in addition to the other spatial dimensions. This arrangement leads to a one-way propagation of a BPM-style approach. The advantage of this mechanism is to allow the numerical time window to follow the evolution of the pulse and, thus, minimize the computer storage of the problem as well as the execution time. The new nonparaxial operator uses the recently developed rational complex coefficient approximation of the well-known Padé approximant to break the paraxial limitation [31]–[34]. Although the resulting numerical operator is an implicit equation, this gives a very robust and stable operator that enables the propagation of ultrashort optical pulses in different geometries. One major advantage of using the Padé approximant operator is that it allows evanescent modes to properly be eliminated by simply rotating the original real-axis branch cut through an angle. It is to be said that implicit techniques are usually very stable as compared to conditionally stable explicit techniques, where some of these explicit methods lose their stability criterion and become unconditionally unstable when new features are added to the problem, such as a perfectly matched layer (PML) or metallic layers [23]. An early result of the new TD–BPM operator has been reported briefly in quick communications using 1-D and homogenous simple models [35], [36]. In this paper, we expand the operator to model ultrashort pulse propagation in dispersive waveguide structures and test the convergence of important numerical parameters. We use this approach to show details of accuracy, efficiency, and stability analysis. In addition, comparisons with the paraxial TD–BPM technique are given thoroughly. For the benefit of convenience, we use a similar verification strategy and analysis used in [22] and [23] for assessment and comparison purposes. In order to highlight fundamental characterization issues of the technique, all structures used in the following analysis have been chosen to have analytical closed-form formulations. In the next section, the new nonparaxial TD–BPM equations will be derived from the wave equation, and the expansion of the operator in terms of the Padé approximant is shown. Section III shows numerical implementations and rigorous testing for the new technique using three different problems. Initially, the technique was examined using propagation of pulsed Gaussian beams in a nondispersive and a homogenous medium, and then, the results were compared with the analytical solution. Second, the method was applied to dispersive linear guided-wave structures of metallic and dielectric waveguides using the propagation of pulsed guided beams. Again, the results were examined against analytical predictions. Additionally, the results of the parabolic TD–BPM were included in all aforementioned analysis for comparison reasons. Section IV shows the application of the new technique to model a practical GaAs directional-coupler structure. A general conclusion is also given at the end of this paper.

II. Theory

We start the formulation of the new technique with the TD wave equation. Assuming a 2-D optical structure (x and z) with the TD wave equation described as

$$\frac{\partial}{\partial_z}\left(r\frac{\partial\psi}{\partial_z}\right)+\frac{\partial}{\partial_x}\left(r\frac{\partial\psi}{\partial_x}\right)=\frac{s}{c_o^2}\frac{\partial^2\psi}{\partial_t^2}. \tag{1}$$

For TE fields, $r=1$, $s=n^2$, and $\psi=E_y$ represents the electric field; for TM fields, $r=1/n^2$, $s=1$, and $\psi=H_y$ represents the magnetic field; c_o is the wave velocity in free space; z is the propagation direction; and $n=n(\mathbf{x})$ is the position-dependent refractive-index variation. It is more convenient to extract a carrier frequency ω and a propagation coefficient $k=k_o n_o$ in the direction of propagation from ψ as

$$\psi=\Psi\exp(-jkz)\exp(j\omega t)+\Psi^*\exp(jkz)\exp(-j\omega t) \tag{2}$$

where $k_o=\omega/c_o$, n_o is a reference refractive index, and $*$ means the complex conjugate. After substitution, (1) can be written in terms of Ψ as

$$r\frac{\partial^2\Psi}{\partial z^2}-2j\left[rk\frac{\partial\Psi}{\partial z}+\frac{s}{c_o}k_o\frac{\partial\Psi}{\partial t}\right]-\frac{s}{c_o^2}\frac{\partial^2\Psi}{\partial t^2}+\frac{\partial}{\partial x}\left(r\frac{\partial\Psi}{\partial x}\right)+(sk_o^2-rk^2)\Psi=0. \tag{3}$$

One of the motivating features of the TD–BPM is the application of the moving time window for efficiency purposes. A compact pulse eventually disappears from the window after a certain number of propagation steps, where it requires the computational window to be adjusted in time at each propagation step. The adjustment, in fact, moves at the group velocity of the pulse envelope. Therefore, the substitution of a moving time coordinate $\tau=t-\nu_g^{-1}z$ with arbitrary ν_g changes (3) to [22], [23], [35], [36]

$$r\frac{\partial^2\Psi}{\partial z^2}-2j\left\{rk\frac{\partial\Psi}{\partial z}+sk_o\left(\frac{1}{c_o}-\frac{1}{\nu_g}\right)\frac{\partial\Psi}{\partial\tau}\right\}-\frac{s}{c_o^2}\frac{\partial^2\Psi}{\partial\tau^2}+\frac{\partial}{\partial x}\left(r\frac{\partial\Psi}{\partial x}\right)+(sk_o^2-rk^2)\Psi=0. \tag{4}$$

To arrive to the parabolic TD–BPM technique equation [22], [23], one can simply neglect the first term in (4) that has the second derivative along the direction of propagation z. On the

other hand, to derive the equation for the wide-angle TD–BPM (Broadband) technique, we define the pseudodifferential square-root operator L given by (5), shown at the bottom of the page at the same time, we can also write (4) in a product form as [31],

$$r\left\{\frac{\partial}{\partial z}-jk_on_o[1-L]\right\}\left\{\frac{\partial}{\partial z}-jk_on_o[1+L]\right\}\Psi=0. \quad (6)$$

We may notice that the first operator in (6) is responsible for forward propagation of the pulse, while the second operator is responsible for the backward propagation. Concentrating on the forward propagation of Ψ, write the formal solution with respect to the initial field $\Psi(0)$ as

$$\begin{aligned}\Psi(z)&=\exp\left\{jk_on_o(1-L)z\right\}\Psi(0)\\&=\exp\left\{jk_on_o(1-\sqrt{1+X})z\right\}\Psi(0).\end{aligned} \quad (7)$$

In the literature, there are a number of approximations for the square-root operator based on Taylor or rational approximation. Recently, a complex rational coefficient approximation based on the well-known Padé approximant was examined rigorously using different applications [31]–[34]. The square-root operator can be approximated as

$$\sqrt{1+X}\approx\prod_{i=1}^{p}\frac{1+g_i^pX}{1+h_i^pX} \quad (8)$$

where g and h are called Padé coefficients, and p is the Padé order. It has been established in scattering problems that evanescent modes are not properly eliminated if real Padé coefficients are used in (8). It was observed that the related error from these modes could be mostly reduced by simply rotating the original real-axis branch cut through an angle [31]–[34]. At the same time, it has also been shown that this technique is equivalent to choosing a complex reference wavenumber [34]. In the following analysis, the FD approach was used as a descritization scheme for both x and τ derivatives. The central difference equations

$$\frac{\partial f}{\partial\alpha}=\frac{f_{m+1}-f_{m-1}}{2\Delta\alpha},\qquad(\alpha=x,\tau) \quad (9\text{-a})$$

$$\frac{\partial^2 f}{\partial\alpha^2}=\frac{f_{m+1}-2f_m+f_{m-1}}{\Delta\alpha^2} \quad (9\text{-b})$$

have been employed to replace the derivatives in (5). Equation (8) was then easily implemented numerically, where the numerator is a simple application on the field, while the denominator was applied using the implicit Gaussian elimination technique. The next section shows the implementations and the characterization of the new technique for modeling ultrashort pulse propagation in a variety of environments.

III. Implementations and Discussions

The new technique described before has been implemented numerically using the Padé approximant operator. In order to characterize the method fully, we apply it to the modelling of ultrashort optical-pulse propagation in different materials and structures. As in the previous analysis, comparisons are made with structures that have closed-form analytical formulation, such as propagation of pulsed optical beams in homogenous and nondispersive material and pulsed guided beams in metallic and dielectric waveguides. In addition, a close assessment with the parabolic-counterpart results will be shown. We try to focus on important numerical parameters that affect convergence, stability, and accuracy. In the following simulations, the input field of the form

$$\Psi(x,z=0,\tau)=\Psi_o(x)G(\tau) \quad (10)$$

has been considered throughout. $G(\tau)$ is the Gaussian pulsed beam of the initial temporal distribution, which is defined as

$$G(\tau)=\exp\left\{-\left(\frac{\tau}{\sigma_{\tau o}}\right)^2\right\} \quad (11)$$

where $\Psi_o(x)$ is the transverse spatial profile of the pulsed beam, and $\sigma_{\tau o}$ scales the duration of the initial pulse in the TD at $z=0$. During numerical simulation, boundary conditions for the optical field are necessary in the transverse spatial and TDs. PML can be used to absorb boundary conditions at the spatial ends of the transverse numerical window. Substituting a lossy spatial coordinate as [37], [38]

$$\hat{x}=x\left(1+i\frac{\sigma_x}{\omega\varepsilon_o n_p}\right) \quad (12)$$

where n_p is the refractive index of the PML medium, which can be chosen to be equal to that of the medium next to the PML layer, and σ_x is the conductivity of the PML layer. In the PML region, the graded conductivity distribution of the form $\sigma_x=\sigma_{\max}(\zeta/\delta)^2$ can be used, where ζ is the distance measured from the interface between the PML layer and the computational space, and δ is the thickness of the PML layer on one side. $\sigma_{\max}$ is the maximum conductivity that can be found by requiring the theoretical reflection coefficient for a plane

$$L=\sqrt{1+X}=\sqrt{\frac{1}{k_o^2n_o^2r}\left\{-2jsk_o\left(\frac{1}{c_o}-\frac{1}{\nu_g}\right)\frac{\partial}{\partial_\tau}-\frac{s}{c_o^2}\frac{\partial^2}{\partial_\tau^2}+\frac{\partial}{\partial_x}\left(r\frac{\partial}{\partial_x}\right)+(sk_o^2-rk^2)\right\}} \quad (5)$$

wave incident on the interface perpendicular to x (PML region) $R(0) = \exp(-2/3n_p\sqrt{\mu_o/\varepsilon_o}\sigma_{\max}\delta)$ to be smaller than a given value [38]. In addition, it is also necessary to compensate for the displacement of the pulse in the time window as the pulse moves forward due to the motion of the envelope Ψ at the group velocity. In practical terms, there are two methods that allow tracking of the time-window movement. The first is called the moving-time-window technique. This technique is simply described by setting zero boundary conditions at the edges of the relative time window (coordinate τ) and moving in the absolute time enclosure (coordinate t) with the group velocity of the pulse. The movement is performed such that the relative motion of the pulse in the time window is eliminated. However, in some complex situations, the desired group velocity ν_g is not known prior to simulation and has to be computed during propagation development. In such a case, a second technique can be used that depends on the idea of periodic boundary conditions. A pulse leaving one side of the relative time window is basically forced to reenter at the other side of the numerical window. Both of these techniques were tested numerically using the new TD–BPM and proved to be very powerful as an efficient numerical tool. One has to note that these techniques are fundamental in terms of saving computer resources, in which they allow the time window to be of a finite amount, which is a multiple of the optical pulsewidths.

A. Homogenous and Nondispersive Medium

The first performance test to be carried out on the new technique involves the propagation of pulsed optical Gaussian beams in a homogenous and nondispersive medium, in which it can be described and compared using a known analytical formulation [39]. One can find the evolution of a pulsed Gaussian beam in homogenous space by taking the inverse Fourier transform of the product of $\widetilde{\Phi}$ and the Fourier transform of the initial pulse that can be written as

$$\Phi(r,\varphi,z,t) = \frac{1}{2\pi}\int_{-\infty}^{\infty} \widetilde{G}(\omega)\widetilde{\Phi}(r,\varphi,z,\omega)e^{-j\omega t}d\omega \qquad (13)$$

where $\widetilde{\Phi}$ is defined in (14), $\widetilde{G}(\omega)$ is the Fourier transform of the initial pulse, and r and φ are the radial and the azimuthal parameters, respectively. Considering a linearly polarized electric field with an initial spatial Gaussian waist w_o at $z = 0$, we can use the well-known frequency-domain representation of an azimuthally symmetric Gaussian beam in a homogeneous medium. The propagation in homogenous space of each frequency component of the spectrum of the wavefunction can be written in the frequency domain as [22], [23], [28], [39]

$$\widetilde{\Phi}(r,\varphi,z,\omega) = \Phi_o\sqrt{\frac{w_o}{w(z)}} \times \exp\left\{j\left[kz - \frac{\eta(z)}{2}\right] - r^2\left[\frac{1}{w^2(z)} - \frac{jk}{2R(z)}\right]\right\} \qquad (14)$$

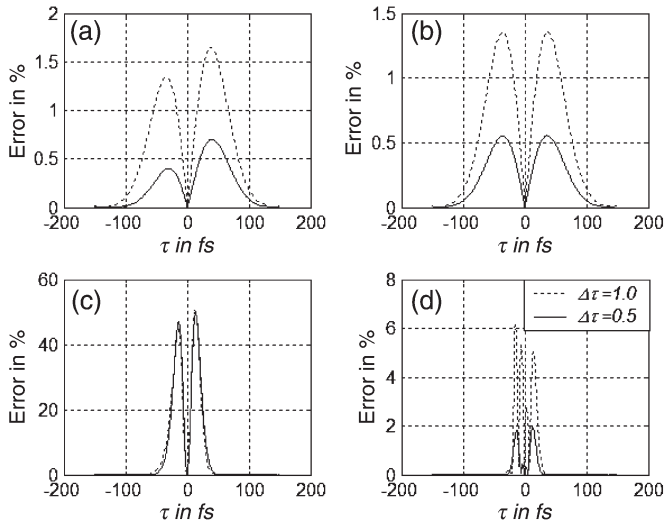

Fig. 1. Percentage error comparison between this technique and the parabolic TD–BPM for different initial short pulsewidths and different time-step sizes. (a) and (c) Parabolic method. (b) and (d) Current technique. (a) and (b) Initial $\sigma_{\tau o} = 50$ fs. (c) and (d) Initial $\sigma_{\tau o} = 10$ fs.

where the waist, the radius of curvature, the phase term, and the diffraction length, respectively, are given by

$$w^2(z) = w_o^2\left[1 + \left(\frac{\lambda z}{\pi w_o^2}\right)^2\right] = w_o^2\left(1 + \frac{z^2}{z_o^2}\right)$$

$$R(z) = z\left[1 + \left(\frac{\pi w_o^2}{\lambda z}\right)^2\right] = z\left(1 + \frac{z_o^2}{z^2}\right)$$

$$\eta(z) = \tan^{-1}\left(\frac{\lambda z}{\pi w_o^2}\right) = \tan^{-1}\left(\frac{z}{z_o}\right)$$

$$z_o = \frac{\pi w_o^2}{\lambda} = \left(\frac{w_o^2}{2c}\right)\omega.$$

The above approach was used to validate results of the new method in this section. For simplicity, the medium was taken to be free space, and the wavelength of the carrier frequency was set as $\lambda = 1.0$ μm. The reference refractive index was chosen to be unity and the initial spatial waist $w_o = 2.5$ μm. Fig. 1 shows the percentage-error comparison between the present technique and the parabolic TD–BPM [23] for different initial short pulsewidths and different time-step sizes. The pulse was propagated to a distance of $Z = 30$ μm with $p = 2$, $\Delta z = 0.1$ μm, and $\Delta x = 0.5$ μm. In this case, the group velocity of the optical pulse $\nu_g = c_o$. The same parameters were used for the parabolic technique, except $\Delta z = 0.1$ μm when $\Delta\tau = 1.0$ fs, while Δz was reduced to 0.05 μm when $\Delta\tau = 0.5$ fs to meet the stability condition. For initial pulsewidths of $\sigma_{\tau o} = 50$ fs, both techniques showed similar behavior, in which the error decreases when the time-step size was reduced. These are shown in Fig. 1(a) and (b). However, Fig. 1(c) and (d) shows a diverse behavior for a smaller initial pulse of $\sigma_{\tau o} = 10$ fs, where the parabolic results are not affected by the reduction of the time-step size with an error around 50%. The reason for

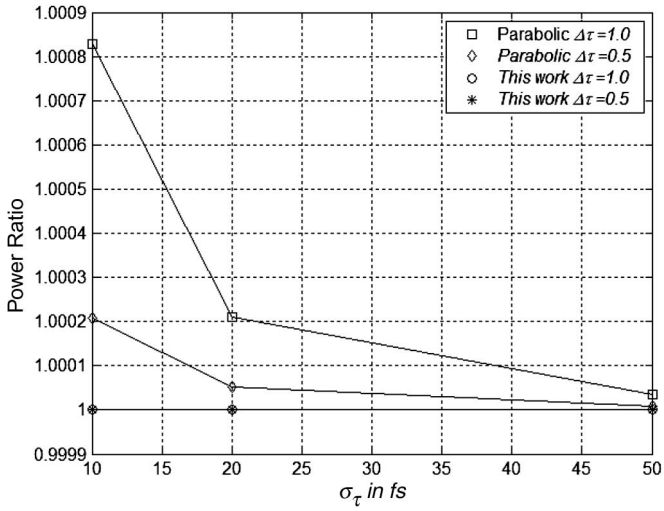

Fig. 2. Power ratios comparison between this technique and the parabolic TD–BPM for different initial short pulse propagation and different time-step sizes. Other parameters are the same as those of Fig. 1.

this is that the paraxial-approximation errors are dominant over the numerical time-step-size errors for ultrashort pulsewidths. On the other hand, the present technique shows that its error depends on the time-step size for ultrashort pulsewidths. It should be understood that, in modeling ultrashort optical pulses, small time-step sizes are needed to represent the rapid variation of the pulse envelope. Fig. 2 shows power ratios in comparison between this technique and the parabolic TD–BPM for the same parameters of Fig. 1. The strong stability of the present technique is clearly demonstrated in the figure shown. Conversely, the figure shows the divergence of the parabolic method, while this divergence is reduced by decreasing the time-step size. However, one has to remember that the reduction of the time-step size is also accompanied by a large reduction in the initial propagation step size for the method to remain stable.

B. Metallic Waveguide

In this section, we examine the new technique for the propagation of ultrashort optical pulses in metallic-waveguide structures. The reason for this choice is that the metallic-waveguide theory has an exact analytical formulation for the measurement of pulse spreading due to dispersion. This will help tune up the numerical parameters of the new method more effectively. Initially, we introduce the theoretical background that is used for verification principles, and then, we show the numerical implementation and comparison between the present technique and the parabolic results. It is known that the propagation of optical beams in a 2-D (x and z) metallic waveguide, with a width of d, gives a cutoff frequency that depends on the width as [23], [40]

$$\omega_c = \frac{i\pi\nu}{d}, \qquad i = 1, 2, 3, \ldots \tag{15}$$

where $\nu = (\varepsilon\mu)^{-1/2}$, and the cutoff wavelength $\lambda_c = 2d/i$, which is measured at the velocity of light in the material between the two metallic-waveguide boundaries. For simplicity, a free-space material between the two mirrors was considered. In this case, the phase velocity of the guided mode is given as

$$\nu_p = \frac{\omega}{\beta} = \frac{\nu}{\sqrt{1-(\omega_c/\omega)^2}} \tag{16}$$

with a propagation constant

$$\beta = \frac{\omega}{\nu}\sqrt{1-(\omega_c/\omega)^2} \tag{17}$$

and the exact group velocity of the pulse beam can be found as

$$\nu_g = \frac{d\omega}{d\beta} = \nu\sqrt{1-(\omega_c/\omega)^2}. \tag{18}$$

Considering a pulsed first guided mode $(i = 1)$ to propagate inside the metallic structure, the temporal pulsewidth, at a distance z, can be measured as [23], [40]

$$\sigma_\tau(z) = \sigma_{\tau o}\sqrt{1+\left(\frac{2z}{\sigma_{\tau o}^2}\frac{d^2\beta}{d\omega^2}\right)^2} \tag{19}$$

where the dispersion term in (19) can be calculated using the following relation:

$$\frac{d^2\beta}{d\omega^2} = \frac{-(\omega_c^2/\omega^3)}{\nu\left[1-(\omega_c/\omega)^2\right]^{3/2}}. \tag{20}$$

We consider the propagation of optical pulses in a waveguide with a width of $d = 1.0$ μm, a cutoff wavelength $\lambda_c = 2$ μm, and a first guided mode in the transverse direction x that can be described as $\Psi_o(x) = \sin(\pi x/d)$. In order to analyze the technique for convergence, stability, and accuracy in this structure, we consider the propagation of a pulsed beam with an initial temporal waist of $\sigma_{\tau o} = 50$ fs and a carrier wavelength of $\lambda = 1.0$ μm. The reference propagation coefficient was chosen to be equal to the propagation coefficient β and $\nu_g = 0.866\ c_o$. Fig. 3 shows the convergence of the technique with the longitudinal step size Δz for different time-step sizes using a Padé order of $p = 2$. The figure shows the percentage-relative time waist error of the pulsewidth, the percentage maximum transverse field error, and the power ratio of the pulsed beam after a distance of $Z = 50$ μm. It is clear from the figure that the technique converges with a longitudinal step size around $\Delta z = 1.0$ μm. The technique also shows very small error in the transverse direction. From Fig. 3, we notice the strong stability of the method with the change of Δz.

Fig. 4 shows the convergence of the technique with the transverse step size Δx for different time-step sizes using different Padé orders of $p = 2$ and 4. The definitions and the parameters are the same of those used in Fig. 3. We notice the convergence of the technique for the two Padé orders used, with the two curves on top of each other. The same conclusion, which is made in Fig. 3, can be observed in this analysis.

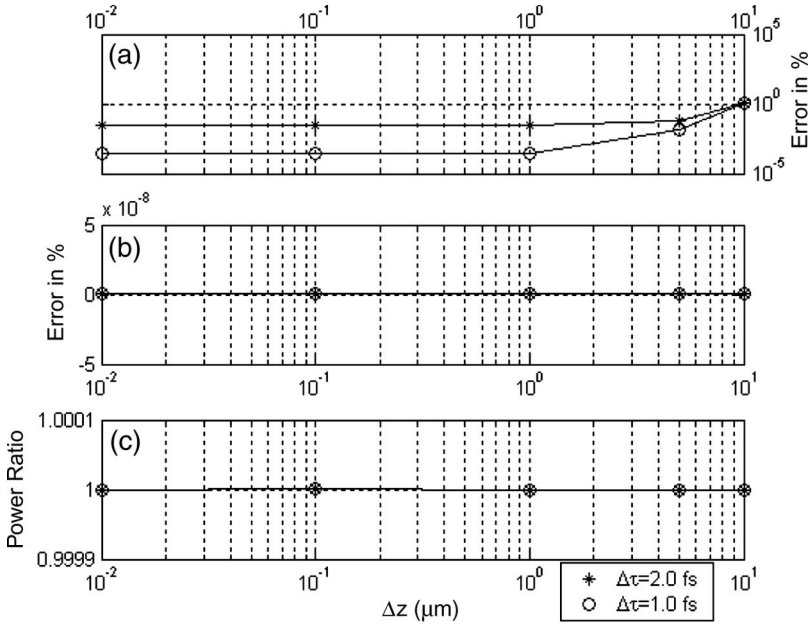

Fig. 3. Convergence of the technique with the longitudinal step size Δz for different time-step sizes. (a) Percentage-relative time waist error. (b) Percentage maximum transverse-field error. (c) Power ratio of the pulsed beam.

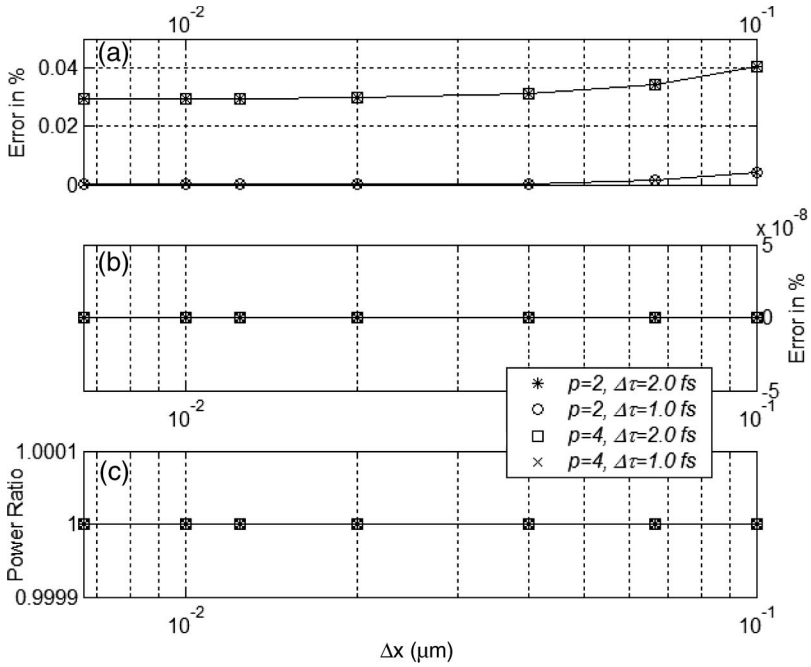

Fig. 4. Convergence of the technique with the transverse step size Δx for different time-step sizes and different Padé orders. (a) Percentage-relative time waist error. (b) Percentage maximum transverse-field error. (c) Power ratio of the pulsed beam.

A comparison between the new technique and the parabolic TD–BPM for different initial short pulse propagation is shown in Fig. 5. The figure shows the percentage-relative time waist error versus the operating-carrier wavelength. The results of the parabolic TD–BPM are those appearing in the study in [23]. The parameters used in these results are $p = 2$, $Z = 332$ μm, $\Delta z = 0.1$ μm, and $\Delta z = 0.01$ μm for the parabolic results. We should notice that increasing the carrier wavelength will increase the propagation angle of the guided plane waves, forming the mode inside the waveguide that can be described as $\theta = \arcsin(\lambda/\lambda c)$, with respect to the axial direction; therefore, this makes the mode less paraxial. In addition, we should also notice that increasing the wavelength decreases the number of carrier cycles under the temporal pulse. It is clear from Fig. 5 that the relative error of the parabolic technique increases by increasing the axial angle. This should be understood, as the error associated with the paraxial approximation becomes more dominant over other errors. The figure also shows that increasing the initial pulsewidth decreases the overall error. Here, it is clear that the paraxial error is reduced due to wider

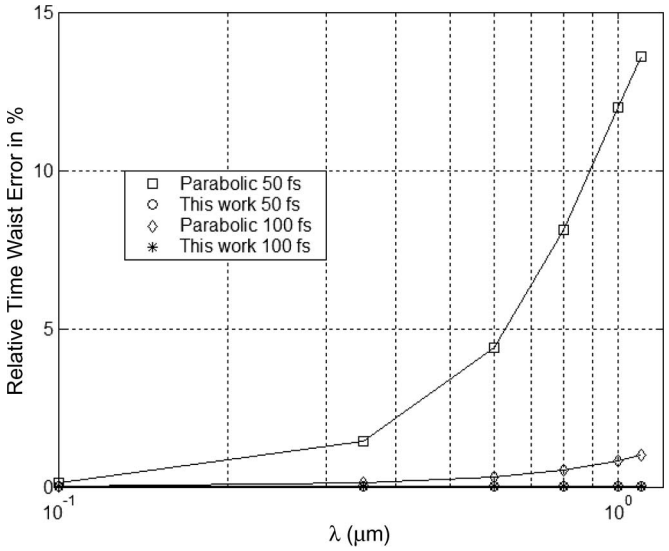

Fig. 5. Comparison between the new technique and the parabolic TD–BPM for different initial short pulse propagation. The percentage-relative time waist error versus the operating carrier wavelength.

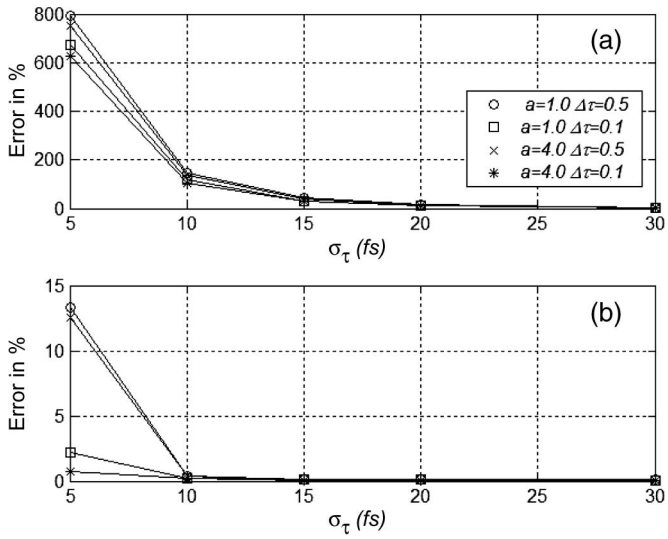

Fig. 6. Comparison between the new technique and the parabolic TD–BPM for different initial ultrashort pulse propagation and different waveguide-core thicknesses a. The percentage-relative time waist error versus the initial time pulsewidth. (a) Parabolic. (b) New technique.

initial optical pulsewidth, which can be interpreted as having more carrier cycles under the pulse envelope. Comparison between the two techniques shows the superiority of the present technique as compared to the parabolic counterpart for both pulsewidths used, in which the errors in both cases are very small and are not affected by the change in λ.

C. Dielectric Waveguide

In this section, we continue the characterization of the new technique by considering the propagation of temporal pulsed optical beams in dielectric waveguides. We assume symmetric-slab waveguides with the following parameters: a core refractive index $n_g = 1.2$, a cladding and a substrate refractive indexes $n_c = n_s = 1.0$, and $\lambda = 1.0$ μm. The waveguide was excited with its respected pulsed first guided mode, and the pulse was propagated to a distance of $Z = 50$ μm with $p = 2$, $\Delta x = 0.2$ μm, $\nu_g = 0.822$ c_o, $\Delta z = 0.1$ μm, and $\Delta z = 0.01$ μm for the parabolic results. The results of the two techniques were verified against the theoretical value of (19), where the dispersion term was computed numerically from the dispersion relation of a dielectric-slab-waveguide theory [23], [41]. Fig. 6 shows a comparison between the new technique and the parabolic TD–BPM for different initial ultrashort pulsewidths $\sigma_{\tau o}$ and different waveguide core thicknesses a. In the figure, the percentage-relative time waist errors versus the initial-time pulsewidths are plotted. One has to note that changing the width of the waveguide modifies the angle of the guided mode with respect to the axial axis. With slab widths of 0.5 and 4.0 μm shown, they correspond to mode angles of 23.7° and 5.3°, respectively. In general, the comparison between the two techniques shows again the superiority of the new technique as compared with the parabolic method for modeling ultrashort pulse propagation in dielectric waveguides. In the case of the parabolic method, it is clear from Fig. 6 that the error connected with the initial pulsewidth is much more obvious than that associated with the mode angle. One has to note again that as

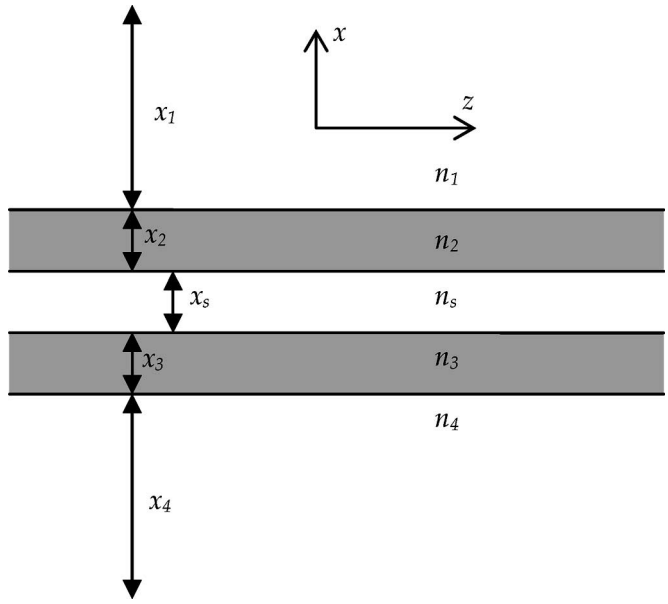

Fig. 7. GaAs directional-coupler structure used in the analysis.

the initial pulsewidth $\sigma_{\tau o}$ decreases, the number of cycles under the temporal pulse also decreases. While the effect of the initial time-step size $\Delta\tau$ is not very critical in case of the parabolic case, but it is shown in the figure that it is very crucial in the case of the new technique. Therefore, we may once again conclude that the error in the new technique is mainly associated with the initial time-step size $\Delta\tau$ rather than the mode angle. It is also understandable from the results of Fig. 6 that ultrashort pulsewidths such as 5 fs require very small time-step sizes to account for the fast variation of the pulse envelope.

The efficiency of the new TD–BPM technique is also quite remarkable for modeling ultrashort pulses; this is in addition to the robust stability and the large propagational step sizes that have been demonstrated in the previous analysis for the variation of numerical parameters. It was observed that the

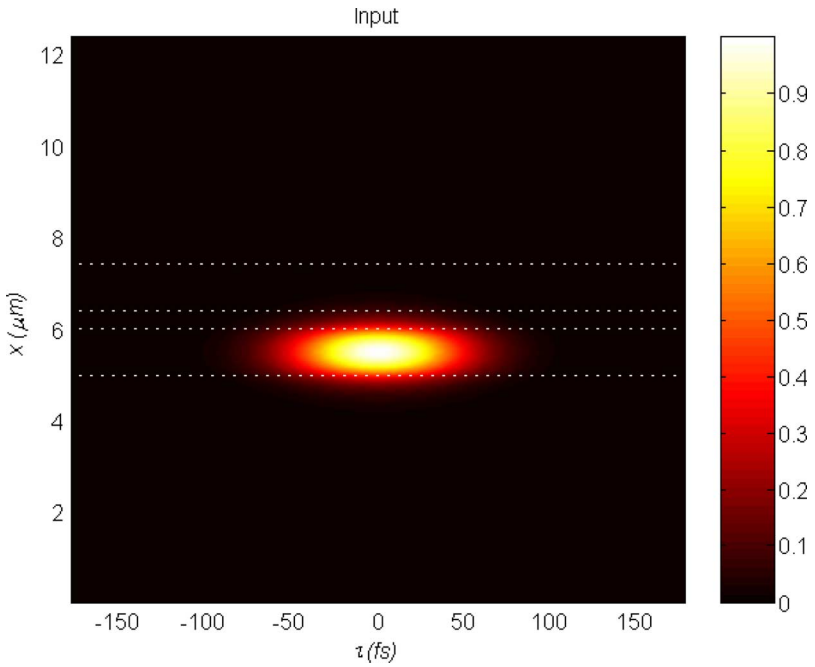

Fig. 8. Input field used in the directional-coupler analysis. The field consists of a pulsed first guided mode of an isolated single waveguide. The two horizontal dotted lines show the position of the two waveguides forming the directional coupler.

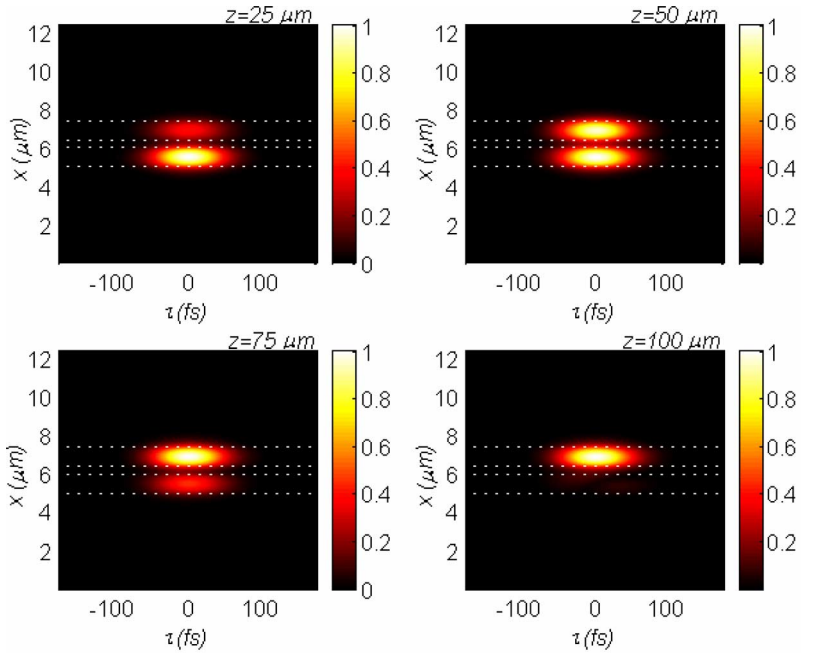

Fig. 9. Evolution of the pulsed optical beam inside the directional-coupler structure at several distances along the longitudinal direction with $x_s = 0.4$ μm, $p = 2$, $\Delta x = 0.05$ μm, $\Delta z = 0.1$ μm, and $\Delta\tau = 2.0$ fs. A moving time window was used to follow the pulse.

technique converges to values around 100 times the values of the explicit FD TD–BPM [23]. The present technique takes around 0.6 s/step when $p = 2$ and 60×150 mesh points of spatial and time discretizations, respectively, while running on an ordinary laptop computer with a 2.1-GHz speed processor. On the other hand, it is known that the parabolic technique is very efficient per propagational step due to the use of the explicit FD approach, but the method is conditionally stable where propagation step size depends inversely on the square of the spatial and the time-step sizes. The decrease of these parameters results in a further reduction in the longitudinal step size with typical values in the range of 0.01 μm.

IV. Application: Directional Coupler

After the establishment of accuracy and stability of the new TD–BPM method in the previous detail analysis, we use the technique to model ultrashort pulse propagation in a GaAs directional-coupler structure, as shown in Fig. 7. The parameters used for the device are as follows: $n_1 = n_s = n_4 = 3.4$,

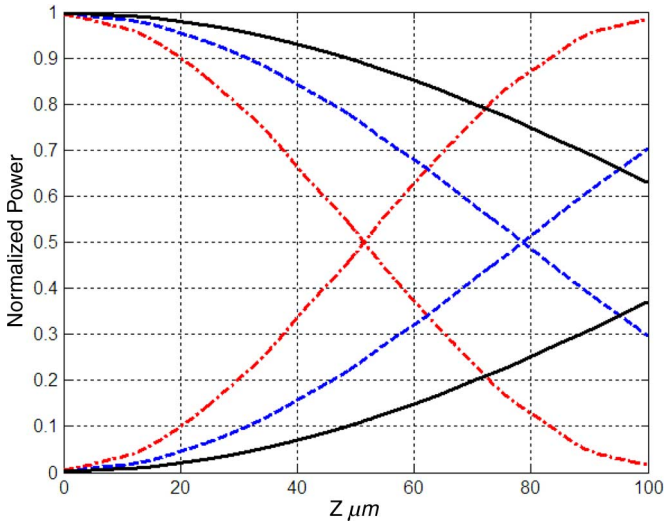

Fig. 10. Normalized power of the two symmetric sides of the spatial window of the directional coupler for different spacing dimensions. Curves starting from one belong to the right half of the spatial window, where the input was excited. Curves starting from zero belong to the left half of the spatial window. Dashed-dotted line is for $x_s = 0.4$ μm, dashed lines are for $x_s = 0.5$ μm, and solid lines are for $x_s = 0.6$ μm. Other parameters are the same as those of Fig. 9.

$n_2 = n_3 = 3.6$, $x_1 = x_5 = 5.0$ μm, $x_2 = x_3 = 1.0$ μm, and $\lambda = 1.55$ μm. The input of the structure was excited with a pulsed first guided mode of the isolated single waveguide with an initial pulsewidth of 50 fs. This field distribution is shown in Fig. 8.

Fig. 9 shows the evolution of the pulsed first guided mode of Fig. 8 inside the directional-coupler device with a waveguide separation $x_s = 0.4$ μm. The figure shows a complete exchange of energy between the two waveguides over a length around 100 μm. Note that the moving-time-window technique was used to follow the pulse propagation with $\nu_g = 0.277c_o$. Fig. 10 shows the normalized power calculated over the two symmetric sides of the spatial window of the directional coupler. In this analysis, the total normalized power of the right-hand side of the spatial window and the left-hand side of the spatial window are plotted for three different separation distances x_s. As expected, when the separation distance between the two waveguides increases, the complete power coupling takes effect over a longer distance.

V. Conclusion

A novel TD–BPM to model long interaction of ultrashort pulsed beams in optical structures has been proposed and analyzed fully. The technique is an extension to the parabolic TD–BPM, which solves the TD wave equation by marching the field along one direction. It uses the Padé approximant to account for the fast envelope pulse propagational variations. The verification process involved comparison with structures that have analytical solutions for rigorous analysis purposes. The technique was validated in homogenous and nondispersive material, metallic and dielectric waveguides, and, later, was applied to a practical optical-communication device. The results of the new technique were also compared systematically with the parabolic TD–BPM. It was concluded that the new method is efficient, very stable, and accurate. It was also observed that the new TD–BPM is particularly well suited to the study of unidirectional propagation of compact temporal pulses over long distances in a guided-wave environment. Future work will include the extension of the technique to examine problems involving material dispersion and nonlinear parametric optical interactions of $\chi^{(2)}$ and $\chi^{(3)}$, where the TD method is essential in order to study the propagation of intense ultrashort pulses.

Acknowledgment

The author would like to thank the University of Toronto, Toronto, ON, Canada, for hosting his sabbatical leave with special appreciation to the host: Prof. J. Setwart Aitchison.

References

[1] K. S. Yee, "Numerical solution of initial boundary value problems involving Maxwell's equations in isotropic media," *IEEE Trans. Antennas Propag.*, vol. AP-14, no. 3, pp. 302–307, May 1966.

[2] A. Taflove, "Review of the formulation and application of the finite-difference time-domain method for numerical modelling of electromagnetic wave infractions with arbitrary structures," *Wave Motion*, vol. 10, no. 6, pp. 547–582, Dec. 1988.

[3] R. W. Ziolkowski and J. B. Judkins, "Full-wave vector Maxwell equation modeling of the self-focusing of ultrashort optical pulses in a nonlinear Kerr medium exhibiting a finite response time," *J. Opt. Soc. Amer. B, Opt. Phys.*, vol. 10, no. 2, pp. 186–198, Feb. 1993.

[4] R. M. Joseph and A. Taflove, "FDTD Maxwell's equations models for nonlinear elctrodynamics and optics," *IEEE Trans. Antennas Propag.*, vol. 45, no. 3, pp. 364–374, Mar. 1997.

[5] R. W. Ziolkowski, "The incorporation of microscopic material models into the FDTD approach for ultrafast optical pulse simulations," *IEEE Trans. Antennas Propag.*, vol. 45, no. 3, pp. 375–391, Mar. 1997.

[6] H. A. Jamid and S. J. Al-Bader, "Finite-difference time-domain approach to nonlinear guided waves," *Electron. Lett.*, vol. 29, no. 1, pp. 83–84, Jan. 1993.

[7] W. P. Haung, S. Chu, A. Goss, and K. Chaudhuri, "A scalar finite-difference time-domain approach to guided-wave optics," *IEEE Photon. Technol. Lett.*, vol. 3, no. 6, pp. 524–526, Jun. 1991.

[8] S. Chu and K. Chaudhuri, "A finite-difference time-domain method for the design and analysis of guided-wave optical structures," *J. Lightw. Technol.*, vol. 7, no. 12, pp. 2033–2038, Dec. 1989.

[9] F. Ma, "Slowly varying envelope simulation of optical waves in time domain with transparent and absorbing boundary conditions," *J. Lightw. Technol.*, vol. 15, no. 10, pp. 1974–1985, Oct. 1997.

[10] R. Y. Chan and J. M. Liu, "Time-domain wave propagation in optical structure," *IEEE Photon. Technol. Lett.*, vol. 6, no. 8, pp. 1001–1003, Aug. 1994.

[11] J. Zhenle, F. Junmei, and F. Enxin, "An explicit and stable time-domain method for simulation wave propagation in optical structures," *Microw. Opt. Technol. Lett.*, vol. 14, no. 4, pp. 249–252, Mar. 1997.

[12] P. Liu, Q. Zhao, and F. Choa, "Slow-wave finite-difference beam propagation method," *IEEE Photon. Technol. Lett.*, vol. 7, no. 8, pp. 890–892, Aug. 1995.

[13] G. H. Jin, J. Harari, J. P. Vilcot, and D. Decoster, "An improved time-domain beam propagation method for integrated optics components," *IEEE Photon. Technol. Lett.*, vol. 9, no. 3, pp. 348–350, Mar. 1997.

[14] J. Shibayama, T. Takahashi, J. Yamauchi, and H. Nakano, "Efficient time-domain finite-difference beam propagation methods for the analysis of slab and circular symmetric waveguides," *J. Lightw. Technol.*, vol. 18, no. 3, pp. 437–442, Mar. 2000.

[15] M. Koshiba, Y. Tsuji, and M. Hikari, "Time-domain beam propagation method and its application to photonics crystal circuits," *J. Lightw. Technol.*, vol. 18, no. 1, pp. 102–110, Jan. 2000.

[16] J. Shibayama, A. Yamahira, T. Mugita, J. Yamauchi, and H. Nakano, "A finite-difference time-domain beam-propagation method for TE- and TM-wave analyses," *J. Lightw. Technol.*, vol. 21, no. 7, pp. 1709–1715, Jul. 2003.

[17] J. Shibayama, M. Muraki, J. Yamauchi, and H. Nakano, "Comparative study of several time-domain methods for optical waveguide analyses," *J. Lightw. Technol.*, vol. 23, no. 7, pp. 2285–2293, Jul. 2005.

[18] M. D. Feit and J. A. Fleck, "Light propagation in graded-index optical fibers," *Appl. Opt.*, vol. 17, no. 24, pp. 3990–3998, Dec. 1978.
[19] H. J. W. M. Hoekstra, "On beam propagation methods for modelling in integrated optics," *Opt. Quantum Electron.*, vol. 29, no. 2, pp. 157–171, 1997.
[20] D. Yevick, "A guide to electric field propagation techniques for guided-wave optics," *Opt. Quantum Electron.*, vol. 26, no. 3, pp. 185–197, Mar. 1994.
[21] Y. Chung and N. Dagli, "Analysis of Z-invariant and Z-variant semiconductor rib waveguides by explicit finite difference beam propagation method with nonuniform mesh configuration," *IEEE J. Quantum Electron.*, vol. 27, no. 10, pp. 2296–2305, Oct. 1991.
[22] H. M. Masoudi, M. A. AlSunaidi, and J. M. Arnold, "Time-domain finite-difference beam propagation method," *IEEE Photon. Technol. Lett.*, vol. 11, no. 10, pp. 1274–1276, Oct. 1999.
[23] H. M. Masoudi, M. A. AlSunaidi, and J. M. Arnold, "Efficient time-domain beam propagation method for modelling integrated optical devices," *J. Lightw. Technol.*, vol. 19, no. 5, pp. 759–771, May 2001.
[24] H. M. Masoudi and J. M. Arnold, "Parallel beam propagation methods," *IEEE Photon. Technol. Lett.*, vol. 6, no. 7, pp. 848–850, Jul. 1994.
[25] H. M. Masoudi and J. M. Arnold, "Parallel three-dimensional finite-difference beam propagation methods," *Int. J. Numer. Model.*, vol. 8, no. 2, pp. 95–107, Mar./Apr. 1995.
[26] H. M. Masoudi and J. M. Arnold, "Parallel beam propagation method for the analysis of second harmonic generation," *IEEE Photon. Technol. Lett.*, vol. 7, no. 4, pp. 400–402, Apr. 1995.
[27] H. M. Masoudi and J. M. Arnold, "Modeling second-order nonlinear effects in optical waveguides using a parallel-processing beam propagation method," *IEEE J. Quantum Electron.*, vol. 31, no. 12, pp. 2107–2113, Dec. 1995.
[28] L. L. Bravo-Roger, M. Zamboni-Rached, K. Z. Nobrega *et al.*, "Spatio-temporal finite element propagator for ultrashort optical pulses," *IEEE Photon. Technol. Lett.*, vol. 16, no. 1, pp. 132–134, Jan. 2004.
[29] A. Bamberger, B. Engquist, L. Halpern, and P. Joly, "Higher order paraxial wave equation approximations in heterogeneous media," *SIAM J. Appl. Math.*, vol. 48, no. 1, pp. 129–154, 1988.
[30] M. D. Collins, "Applications and time-domain solution of higher-order parabolic equations in underwater acoustics," *J. Acoust. Soc. Amer.*, vol. 86, no. 3, pp. 1097–1102, Sep. 1989.
[31] F. A. Milinazzo, C. A. Zala, and G. H. Brooke, "Rational square-root approximations for parabolic equation algorithms," *J. Acoust. Soc. Amer.*, vol. 101, no. 2, pp. 760–766, Feb. 1997.
[32] H. El-Refaei, D. Yevick, and I. Betty, "Stable and noniterative bidirectional beam propagation method," *IEEE Photon. Technol. Lett.*, vol. 12, no. 4, pp. 389–391, Apr. 2000.
[33] P. L. Ho and Y. Y. Lu, "A stable bidirectional propagation method based on scattering operators," *IEEE Photon. Technol. Lett.*, vol. 13, no. 12, pp. 1316–1318, Dec. 2001.
[34] H. Rao, M. J. Steel, R. Scarmozzino, and R. M. Osgood, Jr., "Complex propagators for evanescent waves in bidirectional beam propagation method," *J. Lightw. Technol.*, vol. 18, no. 8, pp. 1155–1160, Aug. 2000.
[35] H. M. Masoudi, "A stable time-domain beam propagation method for modelling ultra short optical pulses," *IEEE Photon. Technol. Lett.*, vol. 19, no. 10, pp. 786–788, May 15, 2007.
[36] H. M. Masoudi, "A novel time-domain technique for nonparaxial ultra short optical pulses," *Microw. Opt. Technol. Lett.*, 2007. To appear.
[37] C. M. Rappaport, "Perfectly matched absorbing boundary conditions based on anisotropic lossy mapping of space," *IEEE Microw. Guided Wave Lett.*, vol. 5, no. 3, pp. 90–92, Mar. 1995.
[38] W. P. Huang, C. L. Xu, W. Lui, and K. Yokoyama, "The perfectly matched layer (PML) boundary condition for the beam propagation method," *IEEE Photon. Technol. Lett.*, vol. 8, no. 5, pp. 649–651, May 1996.
[39] R. W. Ziolkowski and J. B. Judkins, "Propagation characteristics of ultrawide-bandwidth pulsed Gaussian beams," *J. Opt. Soc. Amer. A, Opt. Image Sci.*, vol. 9, no. 11, pp. 2021–2030, Nov. 1992.
[40] S. Ramo, J. Whinnery, and T. V. Duzer, *Fields and Waves in Communication Electronics*. Hoboken, NJ: Wiley, 1984.
[41] D. L. Lee, *Electromagnetic Principles of Integrated Optics*. New York: Wiley, 1986.

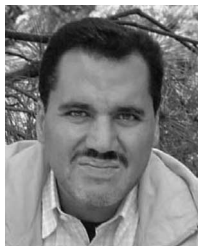

Husain M. Masoudi received the B.S. and M.S. degrees from the Electrical Engineering Department, King Fahd University of Petroleum and Minerals (KFUPM), Dhahran, Saudi Arabia, in 1986 and 1989, respectively, and the Ph.D. degree in optoelectronics from the Electronics and Electrical Engineering Department, University of Glasgow, Glasgow, U.K., in 1995.

In 1995, he was an Assistant Professor with the Department of Electrical Engineering, KFUPM, where, in 2002, he was an Associate Professor. From 1998 to 2004, he was the Manager of the Laser Research Section, Center for Applied Physical Sciences, Research Institute, KFUPM. He was a Visiting Research Professor with several research laboratories and departments, such as the Electronics and Electrical Engineering Department, University of Glasgow, in 1996 and 1998, the Electrical and Electronic Engineering Department, Imperial College of Science, Technology, and Medicine, London, U.K., in 2001, the Institute of Chemical Process Fundamentals, the Czech Academy of Sciences, Prague, Czech Republic, in 2003, and the Emerging Communications Technology Institute, Electrical and Computer Engineering Department, University of Toronto, Toronto, ON, Canada, during the academic year 2006–2007. His academic research interest includes electromagnetic-field interactions with linear and nonlinear materials, optical-fiber communications, and lasers and their applications. His current research interest is in modeling linear and nonlinear optical devices. This includes continuous-wave interactions and pulsed optical beams.